

Experimental investigation of pull loads and borehole pressures during horizontal directional drilling installations

Michael E. Baumert, Erez N. Allouche, and Ian D. Moore

Abstract: Installation loads during 19 commercial horizontal directional drilling (HDD) installations were monitored using new in-hole monitoring cell technology. Fifteen of these installations were part of an 8.3 km section of 203 mm diameter by 4 mm wall thickness steel gas distribution line. The predominant soil type was silty clay, and similar construction practices were employed for all installations. The resistance to pipe advancement within the bore was found to increase in an approximately linear manner, varying from 0.20 to 0.31 kN/m, with a mean of 0.26 kN/m and standard deviation $\sigma_x = 0.03$ kN/m. Local peaks caused by borehole curvature or borehole anomalies were found to dissipate, usually within 10 m, before the underlying linear trend resumed. The remaining four installations were evaluated to determine the relationship between measured pull head load and borehole pressure. The correlation observed provides new insight into the factors that contribute to pulling forces during HDD installations. Based on the findings, a conceptual framework is proposed for an improved HDD design model. The framework outlines two development stages: stage 1, based on tabulated measurements of pulling force per length of pipe inserted; and stage 2, involving significant modifications to an existing prediction model to better represent field conditions.

Key words: pipelines, tensile loads, mud pressure, directional drilling, load monitoring, pressure monitoring.

Résumé : Les charges d'installation au cours de 19 installations de forages directionnels horizontaux commerciaux (HDD) ont été mesurées au moyen d'une nouvelle technologie de cellules de mesure à l'intérieur du trou de forage. Quinze de ces installations faisaient partie d'une section de 8.3 km d'une ligne de distribution de gaz en acier de 203 mm de diamètre et de 4 mm d'épaisseur de paroi. Le type de sol prédominant était de l'argile limoneuse, et des pratiques de construction similaires ont été utilisées pour toutes les installations. On a trouvé que la résistance à l'avancement du tuyau dans le forage augmente d'une façon approximativement linéaire variant de 0.20 kN/m à 0.31 kN/m avec une moyenne de 0.26 kN/m ($\sigma_x = 0.03$ kN/m). On a trouvé que les pics locaux causés par la courbure ou par des anomalies du trou de forage se dissipent, habituellement en deçà de 10 m, avant que la tendance sous-jacente à la linéarité ne reprenne. On a évalué les quatre installations qui restent pour déterminer la relation entre la charge de traction mesurée et la pression dans le forage. La corrélation observée fournit un nouvel éclairage sur les facteurs qui contribuent aux forces de traction durant les installations de HDD. En partant de ces résultats, on propose un cadre conceptuel pour un modèle amélioré de la conception de HDD. Le cadre définit deux stades de développement: stade 1, basé sur les tables de mesures de la force de traction par longueur de tuyau inséré, et stade 2, impliquant des modifications appréciables à un modèle existant de prédiction pour mieux représenter les conditions de terrain.

Mots clés : pipelines, charges de traction, pression de boue, forage directionnel, mesure de charge, mesure de pression.

[Traduit par la Rédaction]

Introduction

Three current design approaches (Drillpath, Driscopipe, and Pipe Research Council International (PRCI)) for predicting tensile pulling loads on pipes installed using horizontal directional drilling (HDD) have been summarized by Baumert

and Allouche (2002), who compared predictions from the three models with rig loads measured in the field during two case histories. Comparison of the measured rig loads with the model load predictions revealed significant inconsistencies in terms of the predicted maximum pulling load value and the rate of load increase with pipe advancement. All three models account for the influence of three parameters, namely surface friction, borehole friction, and the net weight considering pipe buoyancy. In addition, the PRCI model accounts for the bending stiffness of the pipe and the resistance to the advancement of the pipe through a viscous fluid (mud drag). These models provide limited guidance or justification for the selection of input values for the design parameters that govern their predictions.

In the aforementioned case histories, model predictions were compared with loads observed at the drilling rig, as di-

Received 11 March 2003. Accepted 8 September 2003.
Published on the NRC Research Press Web site at
<http://cgj.nrc.ca> on 25 August 2004.

M.E. Baumert and E.N. Allouche. Department of Civil and Environmental Engineering, University of Western Ontario, London, ON N6A 5B9, Canada.

I.D. Moore.¹ GeoEngineering Centre at Queen's-RMC, Queen's University, Kingston, ON K7L 3N6, Canada.

¹Corresponding author (e-mail: moore@civil.queensu.ca).

rect measurements of pipe pulling loads were not available. In subsequent research efforts, monitoring cells were developed to measure actual pull head tensile loads experienced during commercial installations. The first monitoring cells developed at the University of Western Ontario only recorded pull load. Later versions were equipped with pressure transducers to monitor mud pressure in addition to pull loads. The objective of the research reported in this paper is to experimentally examine pull loads during commercial HDD installations to enhance the understanding of the factors that contribute to these loads and to establish the basis for a new empirical design approach for predicting pull loads during HDD installations.

The paper is organized in five major sections. The first section briefly describes the monitoring cells developed at the University of Western Ontario and discusses a representative example of the data that they can provide. The second section describes two datasets: (i) an initial dataset collected with the version of the monitoring cell that measures pulling force only; and (ii) a later, smaller dataset collected with the version of the monitoring cell that measures both pulling force and mud pressure. The third section provides an analysis of the installations in both of these datasets. The fourth section evaluates the Drillpath, Driscopipe, and PRCI models by comparing measured pull loads with model load predictions. Based on the findings, the fifth section proposes a conceptual framework for an improved HDD design model. This section is followed by a closing summary and conclusions.

HDD monitoring cell

General

Three HDD monitoring cells, denoted I, II, and III (Fig. 1), have been developed at the University of Western Ontario. They are inserted into the drill string between the reamer and pipe pull head. Load cell I can be used to measure tensile HDD installation loads of up to 222 kN and downhole mud pressures of up to 690 kPa, with data downloaded from the load cell to a laptop computer at the end of the installation using a conventional cable connection. Load cell II can be used to measure tensile HDD installation loads of up to 36 kN using radio communication to exchange data between the load cell and a laptop computer. Load cell III is designed for measuring loads of up to 670 kN and mud pressures of up to 1034 kPa, relying on a wire transmission line for communication. Load cells II and III both provide real-time data display and complete data download at the end of the installation.

Load cell I was employed on a total of 19 commercial installations. The longest installation monitored was a 226 m installation of 223 mm o.d. and 4.8 mm wall thickness Yellowjacket steel gas distribution pipe. The largest diameter pipe installation monitored was a 152 m installation of 273 mm o.d. schedule 40 Yellowjacket mainline gas pipe. The addition of pressure-monitoring capability is a recent development for this load cell, with four installations monitored to date for combined mud pressure and tensile load.

Load cell II was utilized on six small installations, primarily 51 mm o.d. high-density polyethylene (HDPE) gas line. Because of its load limitation of 36 kN, this load cell is re-

Fig. 1. Monitoring cells I, II, and III (top to bottom). Cell III is approximately 1 m long.



stricted to small-diameter installations or relatively short installations of larger pipe.

Load cell III has not yet been trialed in the field. This load cell is sized for rigs of up to 670 kN thrust capacity and is scheduled for use on two river crossings in March 2003, namely 400 m and 600 m crossings of 406 mm schedule 40 steel pipe.

Downloaded data from all load cells can be easily presented in graphical form for post-installation analysis. Compared to load cell II, the data collected with load cell I are more significant in terms of the magnitude of the recorded loads, the size and length of pipe pulled, and the availability of pressure data. Consequently, subsequent sections of this paper focus on the data collected using load cell I.

Data description

Figure 2 is a graph of the data downloaded after the completion of a typical installation using load cell I (pull load only). The 157 m bore was relatively straight and level to an average depth of 1.2 m in silty clay soil (CL according to the Unified Soil Classification System or USCS). Pull load data were collected at 10 s intervals. A number of observations can be made from Fig. 2. The peaks represent data recorded during rod pullback, and the low points correspond to readings taken when the drill string was stationary as drill rods were being transferred to the rack. There are 52 peaks on the graph corresponding to the 52 drill rods pulled back. The load on the pull head increased linearly with the length of pipe in the bore, at a gradient of approximately 0.28 kN/m, with a maximum load exerted on the pipe of 50.4 kN towards the end of the pull.

Figure 3 is a graph of the mud pressure data downloaded after the completion of a bore using load cell I equipped with a 19 mm diameter pressure transducer having a working range of 0–689 kPa. Pull load data were also collected on this installation and were similar to those shown in Fig. 2. The 155 m bore was relatively straight and level, to an average depth of 1.2 m in clay. Mud pressure data were collected at 10 s intervals. Drilling mud is pumped through the drill string to the reamer during rod pullback, with flow halted during drill rod removal (pumping pressure = 0 kPa). The graph reflects this, with peaks representing mud pres-

Fig. 2. Typical monitoring cell pull load data for pull 9 (157 m, silty clay, 1.2 m depth, 204 mm o.d. 4.8 mm wall steel pipe).

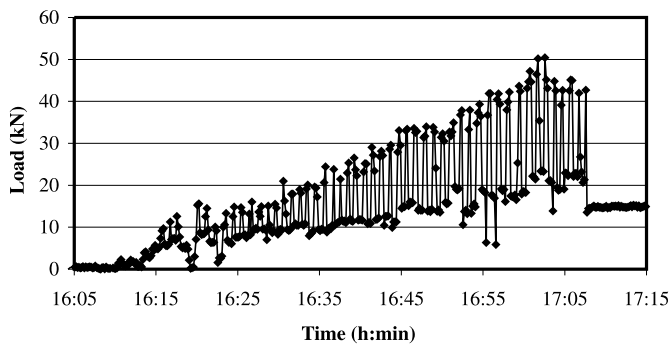
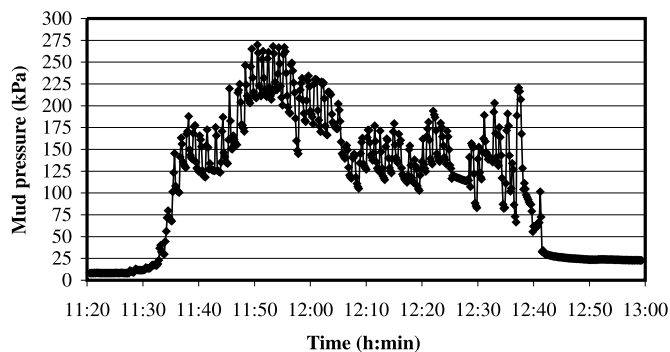


Fig. 3. Typical monitoring cell mud pressure data for pull 18 (155 m, clay, 1.2 m depth, 273 mm o.d. schedule 40 steel pipe).



pressures recorded during rod pullback with active pumping pressure and the low points corresponding to readings taken while drill rods were being transferred to the rack and mud flow was halted. These lows are well above zero, indicating that the bore remains pressurized once mud pumping pressure ceases. There are 50 peaks on the graph corresponding to the 50 drill rods pulled back. The highest mud pressure recorded was 270 kPa and occurred during the early stages of the pull.

Installations monitored for pull load

Data collection

Over a period of 2 months, data were collected with load cell I on 15 commercial HDD installations of 203 mm nominal diameter (4.8 mm wall thickness, weight 25.34 kg/m) Yellowjacket steel gas pipe. The data, summarized in Table 1, make up a unique set of HDD installations along the path of an 8.3 km section of gas-distribution line in a rural area. The majority of the gas line installation was completed by conventional open cut, and HDD was employed, where necessary, to traverse drainage ditches, creeks, and tree lines along the gas line right-of-way and to avoid disturbing landscaped residential and commercial property frontage. The ground surface was roughly level for 12 of the 15 installations, with the pipe installed at an average depth of 1.2 m to crown below the surface. The remaining three installations were crossings of depressions (one creek crossing and two drainage ditch crossings; Table 1, pulls 13, 14, and 15, respectively). All installations were conducted by the same drilling crew using a Vermeer 24 × 40 drill rig. With one ex-

ception, discussed later, the drilling practice employed was similar for all installations. The procedure consisted of (i) a mud mix of water mixed with Tru-Bore, a highly concentrated bentonite drilling product, and Pro-Pac, a polymer additive that promotes borehole stability; (ii) drilling of a 102 mm pilot bore; (iii) prereaming with one pass of a 356 mm diameter fluted Vermeer reamer; (iv) advancing the drill string with the reamer attached, back through the pre-reamed bore (no rotation); (v) attaching the load cell between the reamer and pipe pull head; and (vi) pulling the pipe product, supported on rollers, back through the pre-reamed bore. For the horizontal installations, significant pipe curvature occurred only at the entry side of the bore where the pipe, over the distance of the slip trench, descended from the level of the rollers to the 1.2 m depth of the bore. At the exit end the pull was terminated three rod lengths (9.1 m) short of the rig, where an exit pit was dug and the pipe was disconnected from the drill stem. This procedure left the pipe in a horizontal inclination at a depth of 1.2 m, ready for connection (tie in) to the next section of pipe. The creek crossing (Table 1, pull 13) was bored to pass 2 m below the creek bed. The first attempt at crossing the field drainage ditch (Table 1, pull 14) was bored 3 m below the ditch bottom. When this installation failed during pullback as a result of pipe jamming, a second, successful, attempt (Table 1, pull 15) was bored 4.5 m below the ditch bottom.

During pipe pullback, manual recordings were made of the drill rig gauge readouts. The following gauge readouts during the pullback of each rod were recorded: (i) maximum pull, and (ii) maximum mud pressure. The timing (start and finish) of each rod pulled was also manually recorded to aid in the correlation of pull data to length of pipe installed. All rods were 3.048 m in length. The rig gauge pull readings were recorded for later comparison with monitoring cell data to evaluate the accuracy of rig loads as a measure of the actual load exerted on the pipe product. At the end of each pull, pull data were downloaded from the load cell onto a laptop computer for display and post-installation analysis. Soil samples were taken from the entry and exit pits.

Soils analysis

Table 1 presents a summary of the 15 installations conducted, including length of installation (m), maximum pull load recorded by the monitoring cell (kN), pulling force gradient (kN/m), pullback rate (m/min), predominant soil type encountered, and proportion of clay size particles. A quick study of the table indicates that silty clay (CL) was the predominant soil type encountered for 12 of the installations. Field classification was conducted for pulls 10, 11, and 12 (Table 1), identifying these soils as silty clay. For the three depression crossings, pulls 13–15 (Table 1), the soil also included a significant gravel and sand component (GW and GC, according to the USCS) at one end of the installation, with CL encountered at the other. Figure 4 presents the grain-size distribution derived from a standard sieve analysis test (ASTM 1998a, 1998b) for pulls 1–9 (Table 1) completed in silty clay. Figure 5 presents the grain-size distribution for the coarse soils encountered in pulls 13–15 (Table 1). The dataset of 15 installations was divided into two groups for subsequent analysis. The first group (pulls 1–12) comprises 12 level profile installations in silty clay; the

Table 1. Monitoring cell I: pull load measurements from 15 commercial installations.

Pull No.	Length (m)	Max load (kN)	Gradient (kN/m)	Intercept (kN)	Pullback rate (m/min)	Soil classified according to the Unified Soil Classification System and ASTM (1998a, 1998b)	
						Clay-size particles (%)	
1	146	40.5	0.138	17.7	5.5	CL: lean silty clay with 14% sand and fine gravel	19
2	226	53.8	0.164	7.9	4.9	Entry, CL: lean silty clay with 22% sand and gravel Exit, CL: lean silty clay with 22% sand and gravel	31 29
3	122	40.3	0.169	12.7	4.6	CL: lean silty clay with 9% sand and fine gravel	26
4	152	45.0	0.197	5.2	5.5	CL: lean silty clay with 18% sand and fine gravel	18
5	174	58.4	0.229	11.5	7.3	CL: lean silty clay with 7% fine sand	24
6	64	19.9	0.233	3.2	8.3	CL: lean silty clay with 30% sand and gravel	20
7	110	33.4	0.239	1.7	8.7	CL: lean silty clay with 25% sand and gravel	23
8	183	65.3	0.269	7.0	4.8	Entry, CL: low-plasticity silty clay with 46% sand and gravel Exit, CL: lean silty clay with 9% fine sand	10 22
9	157	50.4	0.281	2.6	6.5	CL: lean silty clay with 30% sand and gravel	20
10	91	28.3	0.117	13.2	6.3	CL (field classification)	—
11	76	23.2	0.213	5.0	5.5	CL (field classification)	—
12	66	15.9	0.110	8.5	3.0	CL (Field classification)	—
13	122	62.0	0.360	3.2	2.3	Entry, GC: well-graded gravel – sand – silty clay mixture (fines 48%) Exit, CL: lean silty clay with 13% sand and fine gravel	— 33
14	58	91.4	0.976	11.4	1.7	Entry, GW: well-graded gravel–sand mixture with little fines Exit, CL: lean silty clay with traces (3%) sand and fine gravel	— 35
15	94	27.9	na	na	8.0	Entry, CL: lean silty clay with traces (3%) sand and fine gravel Exit, GW: well-graded gravel–sand mixture with some silty fines (fines 18%)	35 —

Note: Pulls 13–15 are depression crossings, and pulls 1–12 are level profile installations. na, not available.

Fig. 4. Fine soil grain-size distributions (pulls 1–9, Table 1).

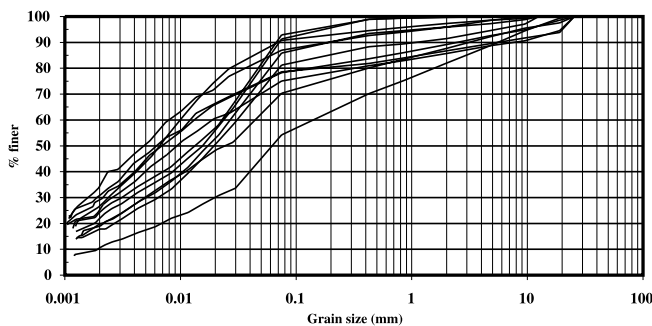
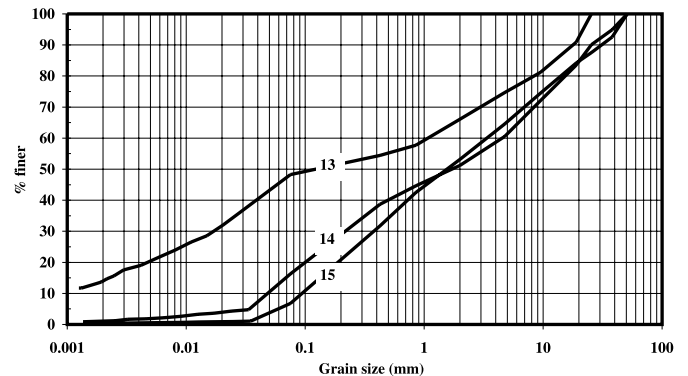


Fig. 5. Coarse soil grain-size distributions (pulls 13–15, Table 1).



second group, the three depression crossings (pulls 13–15), were completed in mixed soil conditions. The first group is unique in that it provides the opportunity to study the load response of a particular pipe type of given diameter installed in one predominant soil condition. The second group is instructive because it is indicative of the higher loading associated with coarser soil conditions relative to silty clay. These installations also highlight the impact of construction practice, as will be discussed in a later section.

Level profile installations in silty clay

Baseline linear trend

The load cell data for each installation were analyzed us-

ing standard statistical tools. The data were divided into two separate datasets for each pull, one set collecting the data points recorded during active rod pullback, the second set collecting data points recorded while the drill stem was stationary (during rod removal to the storage rack). A linear regression was then conducted for the active rod pullback dataset. Table 1 (pulls 1–12) summarizes the results for group one (12 level profile installations in silty clay). Figure 6 represents a typical installation in this group (Table 1, pull 4). The regression for active rod pullback for this installation yields a gradient of 0.20 kN/m with an intercept of 5.24 kN ($R^2 = 0.75$). The standard deviation is $\sigma_x = 4.90$ kN.

Fig. 6. Five local pull load peaks are identified for pull 4 (152 m, silty clay, 1.2 m depth, 204 mm o.d. 4.8 mm wall steel pipe).

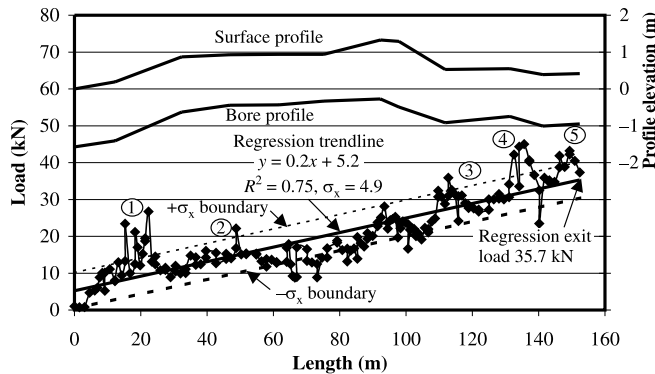


Table 2. Bore resistance: 12 level profile installations in silty clay (CL).

Pull No.	Length (m)	Actual max load near exit (kN)	Regression exit load (kN)	Bore resistance (kN/m) ^a
1	146	43.7	37.8	0.259
2	226	53.8	45.0	0.199
3	122	40.3	33.3	0.273
4	152	45.0	35.2	0.232
5	174	58.4	51.4	0.295
6	64	19.9	18.1	0.283
7	110	33.4	28.0	0.254
8	183	65.3	56.3	0.307
9	157	50.4	46.7	0.298
10	91	28.6	23.7	0.261
11	76	23.2	21.2	0.279
12	66	15.9	15.8	0.239

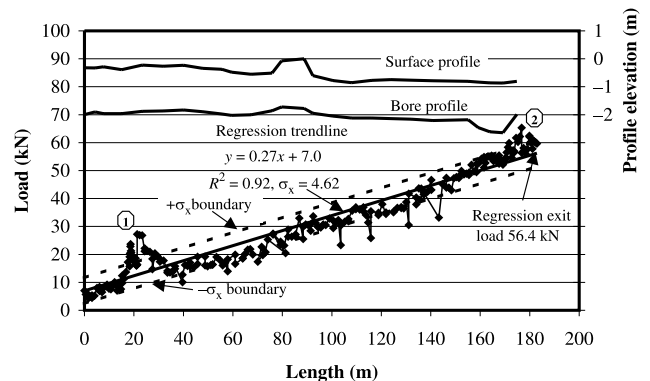
Note: Mean bore resistance for bores 1–11 is $m_x = 0.26$ kN/m, with a standard deviation of $\sigma_x = 0.03$.

^aCalculated as (regression exit load)/(total bore length).

In Table 2 the regression load at the end of the pull for each installation was calculated by multiplying the regression slope (Table 1, column 4) by the length of the pull and adding the initial offset (Table 1, column 5). The result is referred to in Table 2 as the regression exit load. Figure 6 identifies the regression exit load for pull 4. The load recorded at the pull head when the pipe exits the bore can be entirely attributed to resistance to pipe advancement within the bore, as there is no pipe at the surface to contribute to surface drag. To obtain an average value for the resistance to pipe advancement per unit length of pipe within the bore, the regression exit load was divided by the total bore length. These values are listed in Table 2 under the heading bore resistance (kN/m). For the 12 level installations completed in silty clay, the bore resistance varies from a low of 0.20 kN/m for bore 2 to a high of 0.31 kN/m for bore 8. The mean bore resistance for these installations is $m_x = 0.26$ kN/m, with a standard deviation of $\sigma_x = 0.03$ kN/m.

The bore resistance represents that component of the total load measured by the monitoring cell that can be attributed solely to the section of pipe within the bore. The resulting narrow distribution of 0.26 ± 0.06 kN/m for 12 installations

Fig. 7. Two local pull load peaks are identified for pull 8; the first peak does not appear to be associated with a change in borehole curvature (183 m, silty clay, 1.2 m depth, 204 mm o.d. 4.8 mm wall steel pipe).



in silty clay is significant in that it indicates that it may be feasible to refine load predictions as a function of the predominant installation soil type, a possibility that will be discussed later in this paper.

Peak analysis

For each level profile installation completed in silty clay, the baseline linear trend is modulated by local peaks. The peaks tend to dissipate with the underlying load response returning to a baseline linear trend. For analysis purposes, “peaks” were defined as a grouping of load readings possessing a discernable peak formation whose local maxima exceeded the underlying baseline linear trend by at least one standard deviation, σ_x . Multiple peaks occurring in close proximity to one another were grouped together as one peak formation likely having the same underlying cause. In Fig. 6 (Table 1, pull 4), five peaks that met this criterion were identified (the peak at roughly 95 m, between peaks 2 and 3, fell below the $+\sigma_x$ boundary and was therefore not included). These peaks roughly correlate with changes in borehole curvature. In a theoretical parametric study of the effects of bore-path profile, Polak and Chu (2002) found pull loads to be particularly sensitive to double-curvature effects. Other peaks occur that do not appear to be associated with a change in borehole curvature such as the first peak in Fig. 7 (Table 1, pull 8). Such peaks are likely caused by random obstructions in the borehole path such as boulders, cobbles, or partial borehole collapse. All peaks observed dissipated and do not significantly affect the long-term baseline linear trend. A statistical analysis was conducted on the 43 peaks that met the previously stated definition. An average peak in this dataset has an amplitude of 10.3 kN ($\sigma_x = 1.0$ kN) and duration, start to finish, of 9.3 m ($\sigma_x = 0.8$ m).

Start peaks

In three out of the 12 installations, significant peaks occurred at the beginning of the installation with less than 15 m of pipe in the ground. Table 3 summarizes the properties of the start peaks for these three installations, providing their magnitude (kN), position (m), and length (m). For comparison, the actual maximum load at the end of the installation (kN) is also listed. The magnitude of these start peaks can be significant, since they approach or even exceed

Table 3. Start peaks.

Pull No.	Bore length (m)	Start peak magnitude (kN)	Actual max load near exit (kN)	Position along borehole (m)	Length of peak (m)
1	146	37.9	43.7	9.1	9.1
2	226	24.9	53.8	13.2	30.5
10	91	28.6	28.3	6.7	8.4

Table 4. Depression crossings.

Pull No.	Length (m)	Max load near exit (kN)	Regression exit load (kN)	Bore resistance (kN/m) ^a
13	122	62.0	47.1	0.386
14	61.0	80.5	68.0	1.172
15	94.5	27.9	na	0.295 ^b

Note: Pulls 14 and 15 cross the same ditch. Pull 14 was the first attempt and it failed. Pull 15 was the second attempt and it was successful. na, not available.

^aCalculated as (regression exit load)/(total bore length).

^bCalculated as (maximum exit load)/(total bore length).

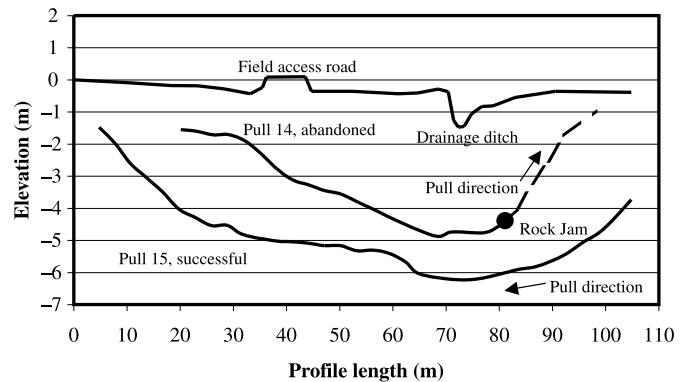
the pull load recorded at the end of the pull which would otherwise be expected to be the maximum recorded load. These peaks may be attributable to installation practice. The authors suspect that the slip trenches at the pipe entrance pits were, in these cases, too short and steep, presenting an entrance borehole profile with excessive curvature that made it difficult for the pipe to navigate cleanly. Alternatively, the borehole at the entrance to these installations may have been partially collapsed or not sufficiently cleared of drill cuttings. In a section presented later in this paper covering mud pressure monitoring, it was found that mud pressure can rapidly rise at the start of a bore. This may also contribute to the formation of start peaks as the mud pressure exerts a load on the pull head. Start peaks can likely be minimized through improved construction practice (i.e., digging longer slip trenches, ensuring a clear entrance bore).

Depression crossings: construction effort

The three depression crossings were completed in mixed soil conditions with a significant gravel component. These three crossings are summarized in Table 4. They demonstrate a number of significant points. The most significant is the effect that variation in the type of soil has on the pull load. The 12 pulls completed in silty clay had a mean bore resistance to pipe advancement of 0.26 kN/m ($\sigma_x = 0.03$ kN/m). The higher resistance to pipe advancement associated with the depression crossings presented in Table 4 (0.30–1.17 kN/m) is likely the result of gravelly sand along a portion of the bore path. Soil samples were taken at the entry and exit locations, with coarse soil found at the entry pits and silty clay at the exit pits (pulls 14 and 15). With no samples taken at deeper intermediate points along the profile, the extent of the coarser soil zone was not determined.

Pulls 14 and 15 traversed the same drainage ditch. Pull 14 was terminated and the pipe product was abandoned when the rig reached its capacity after hanging up on a large boulder after completing roughly two-thirds of the pullback. Pull 15 paralleled the first attempt, with a horizontal offset of

Fig. 8. Bore profiles for pulls 14 and 15 (204 mm o.d. 4.8 mm wall steel pipe).



1 m and a deeper profile under the ditch. The profiles are shown in Fig. 8. The setup for the second attempt was reversed with the rig positioned on the opposite side of the ditch pulling in the opposite direction. Additional construction changes were made. The pipe entry slip trench was excavated below the gravel–sand layer so that the pullback began in silty clay. With this arrangement, the gravel–sand layer was encountered towards the end of the pull, with the majority of the pipe already pulled in place. This contrasts markedly with the first attempt where the pipe was initially drawn through the gravel–sand layer. The contractor also slowed both the pre-ream and pullback rates and added a detergent to the drilling fluid to decrease the stickiness of the clay in the bore. These actions improved the quality and cleanness of the borehole. No rock obstructions were encountered on this pullback, and an installation of 94.5 m, 50% greater in length than the first attempt, was completed with a maximum pull of 27.9 kN, roughly one third of the maximum pull load experienced on the first attempt. Figures 9 and 10 show the pull load data for pulls 14 and 15, respectively. Of particular interest is the load record for pull 15 (Fig. 10). The load increases (0.23 kN/m) for the first half of the pull (up to 45 m) and then levels off, with a slight decline (–0.05 kN/m) for the second half of the pull. Essentially, during the second half of the pull, the resistance to pipe advancement per metre encountered in the borehole was marginally less than the ground resistance per metre of pipe remaining at the surface. This section of the pullback was also assisted by the contribution of positive pipe buoyancy in the direction of the pull. It can be inferred that the borehole in the second half of the bore was in excellent condition, stable, and clear of cuttings, with mud drag reduced by the addition of detergent to the drilling mud. This example illustrates the importance of preplanning a bore, i.e., tak-

Fig. 9. Pull load data for pull 14 (61 m, mixed soil conditions, 204 mm o.d. 4.8 mm wall steel pipe).

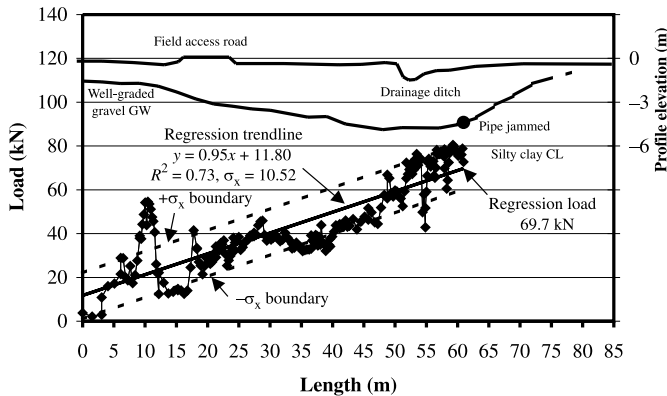
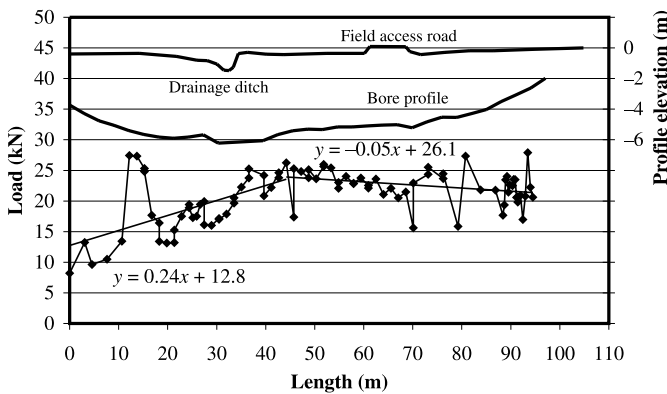


Fig. 10. Pull load data for pull 15 (94.5 m, mixed soil conditions, 204 mm o.d. 4.8 mm wall steel pipe).



ing the time to gather pertinent information and using it to advantage.

Installations monitored for load and mud pressure

General

Mud pressure capability was added to monitoring cell II after data were collected on the 15 pulls described in the previous sections. Mud pressure is a significant parameter from a number of perspectives. From an operational point of view, mud pressure must be maintained within a range with lower and upper limits. The lower limit is controlled by the minimum pressure required to maintain borehole stability and prevent borehole collapse. The upper limit is determined by the pressure that will cause “frac-out,” the inadvertent escape of drill mud out of the bore into the surrounding formation and possibly to the surface (Staheli et al. 1998). Within these limits, the pressure must be high enough to maintain turbulent flow sufficient to transport drill cuttings out of the bore and prevent their settlement to the bottom of the bore. Defining the optimal mud pressure range for a particular bore is a challenge, controlled by fluid mechanics and geotechnical issues, and is beyond the scope of this paper. The discussion that follows focuses on the relationship between pull load and borehole mud pressure and the contribution of the latter to the pull load measured at the pull head.

Dataset: pulling loads and mud pressure

Table 5 summarizes the results of four level profile installations that were monitored for mud pressure and pulling load. The table includes the length of the installations (m), maximum recorded load (kN), maximum recorded pressure (kPa), in-bore pipe resistance (kN/m), predominant soil type encountered, and a description of the pipe product installed and downhole equipment used. Pulls 16 and 17 were installations of 203 mm o.d. SDR 11 HDPE pipe, with the ratio of outside diameter to wall thickness (SDR) of 11, and both were conducted in the same clay soil. These two installations paralleled each other, with a horizontal separation of 3 m and virtually identical vertical profiles. Pulls 18 and 19 were mainline gas line installations of 273 mm o.d. schedule 40 steel pipe. Pull 18 was completed in clay, and pull 19 in saturated sand.

Load components measured by monitoring cell

The total pull load as measured by the monitoring cell can be broken down into load components that are accumulated at the surface and those accumulated in the bore: (i) the load accumulated at the surface (surface load) is the resistance to pipe advancement due to surface drag or friction of the portion of pipe that remains at the surface; and (ii) the load accumulated in the bore (bore load) is the pull head pressure load (mud pressure load on the pull head due to the pressurized state of the bore) and the in-bore pipe load (resistance to pipe advancement due to a combination of bore wall friction, fluidic mud drag, and solids drag on the portion of the pipe in the borehole).

The magnitude of these components can be estimated. A characteristic surface friction factor can be calculated based on the known weight of the pipe and the pull load measured when the pipe is initially drawn into the bore (i.e., when the pull load can be entirely attributed to surface friction). The surface load component can be calculated at any stage of the installation once this friction factor is determined. Bore load can then be calculated by subtracting the surface load component from the total load measured by the monitoring cell. The bore load can then be separated into its two components. The pressurized mud in the bore exerts a pressure and hence a force on the face of the pull head, a force that is transferred to the monitoring cell. For example, for pull 16 (Table 5; Fig. 11), the maximum recorded pressure of 374 kPa would exert a force of 17 kN on the pull head (0.254 m diameter, 0.0507 m² projected area). Knowing the measured mud pressure, the pull head pressure load can be calculated for any stage of the installation. The in-bore load can then be calculated by simply subtracting the pull head pressure load from the calculated bore load. The total loads measured by the monitoring cell for pulls 16–19 are broken into their respective components and analyzed in the next section.

Data analysis: pulling loads and mud pressure

Figure 11 displays the total load at the pull head and the pressure data for pull 16 (Table 5). In this graph the mud pressure and total load trends tend to mirror each other, generally rising and falling together. Figure 12 graphs the calculated pull head pressure load and the ratio of the pull head pressure load to the total load measured by the monitoring

Table 5. Pull load and mud pressure monitoring data.

Pull No.	Length (m)	Max pull (kN)	Max pressure (kPa)	In-bore pipe resistance (kN/m) ^a	Soil type	Pipe product	Type of reamer
16	115	25.8	374	0.082	Clay	203 mm SDR 11 HDPE	Barrel
17	118	22.5	280	0.094	Clay	203 mm SDR 11 HDPE	Barrel
18	155	47.3	270	0.180	Clay	273 mm o.d. schedule 40 steel pipe, 60.24 kg/m	Vermeer (356 mm)
19	140	76.5	178	0.414	Fine sand (saturated)	273 mm o.d. schedule 40 steel pipe, 60.24 kg/m	Kodiak (356 mm)

^aPressure component removed.

Fig. 11. Pull load and pressure data for pull 16 (115 m, clay, 220 mm o.d. SDR 11 HDPE pipe).

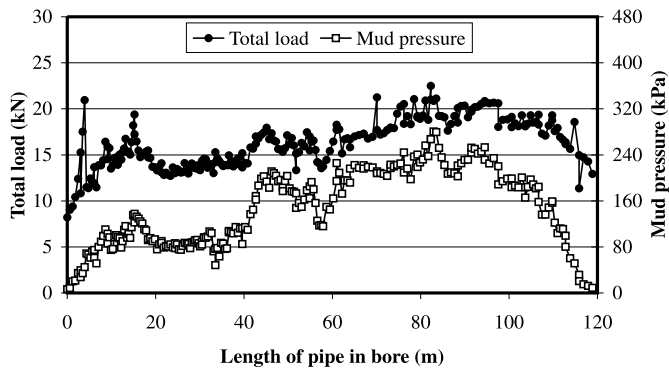
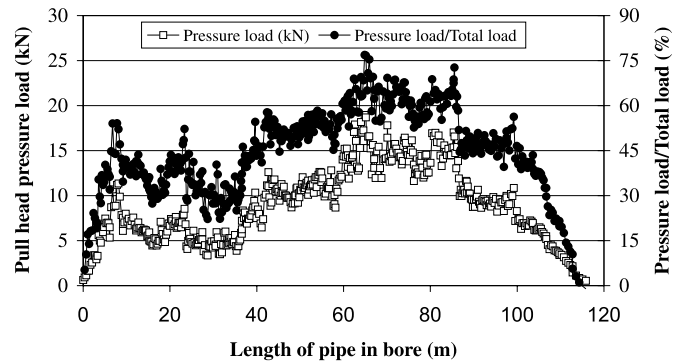
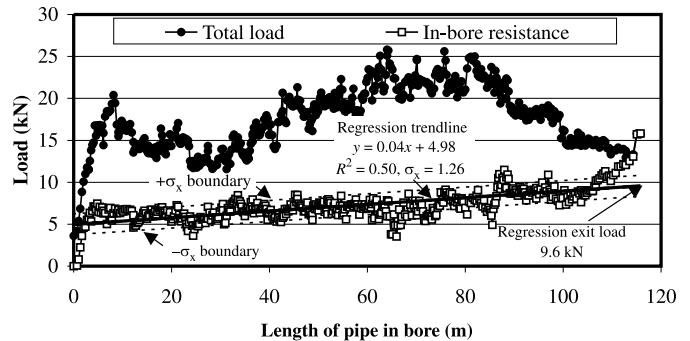


Fig. 12. Pull head pressure load for pull 16 (115 m, clay, 220 mm o.d. SDR 11 HDPE pipe).



cell, both against the length of pipe in the bore. This figure demonstrates that the pull head pressure load, with the exception of the start and exit sections, can form a significant portion (from 25% to as high as 77%) of the total load measured by the monitoring cell. Figure 13 graphs the total load measured by the monitoring cell and the in-bore pipe resistance, both as a function of the length of pipe in the bore. Removal of the surface load and the pull head pressure load components from the total pull load reveals an underlying approximately linear relationship for the in-bore pipe load that is not as apparent when examining the graph of the total load alone. In Fig. 13 this linear trend is indicated and a regression equation is added ($R^2 = 0.50$).

Fig. 13. In-bore pipe resistance for pull 16 (115 m, clay, 220 mm o.d. SDR 11 HDPE pipe).



Similar graphs generated for pulls 17–19 demonstrated a similar near-linear trend for their respective in-bore resistance loads. For the sake of brevity, the results, including pull 16, are summarized in Table 6. Studying this table it is again apparent how sensitive pulling loads are to soil conditions in the borehole. Comparing pulls 18 and 19, the average in-bore pipe resistance encountered for an installation in saturated fine sand (0.414 kN/m, pull 19) was more than twice that encountered for a similar pipe installation in clay (0.180 kN/m, pull 18).

The regression equations calculated for the in-bore pipe resistance for pulls 16 and 17 are similar. This is an expected result because the bore conditions and profiles for the two installations were virtually identical.

For the three pulls completed in clay (16, 17, and 18), the maximum pull head pressure loads (18.9, 14.2, and 15.8 kN, respectively) make up a major component (77%, 66%, and 67%, respectively) of the maximum pull head load measured by the monitoring cell (25.8, 22.5, and 23.9 kN, respectively). For pull 19, the single installation completed in sand, the maximum pull head pressure load of 10.4 kN is still significant but because of the higher total load measured (53.2 kN) it forms a smaller percentage (20%) of the total.

In the four installations presented in this paper that were monitored for pressure (Table 5, pulls 16–18), the pressure was measured in the bore annulus between the reamer and the pull head. No measurements in the bore annulus on the rig side of the reamer were taken. In a study by Staheli et al. (1998), the pressure on the rig side of the reamer was monitored for three 160 m installations of 305 mm o.d. steel pipe. Regardless of the internal nozzle pressures, which were systematically varied, the pressures measured in the bore annulus 0.3 m behind the nozzle were found to lie within a narrow range (324–358 kPa). The significant point to note is that these pressures are significant and exert a pressure on the reamer that is transferred to the drill rig.

Table 6. Mud pressure summary.

Pull No.	Soil	Maximum pull head pressure load				In-bore regression equation (kN)	Bore length (m)	In-bore pipe resistance (kN/m)
		Pressure (kPa)	Load (kN)	Position length	% of total load			
16	Clay	374	18.9	0.45	77	$y = 0.040x + 4.98$	115	0.082
17	Clay	280	14.2	0.70	66	$y = 0.027x + 5.44$	118	0.073
18	Clay	270	15.8	0.28	67	$y = 0.15x + 4.70$	155	0.180
19	Sand	178	10.4	0.63	20	$y = 0.33x + 12.30$	140	0.414

Model comparison

As demonstrated in the previous section of this paper, data collected using the monitoring cell on individual pulls provide a clear record of pipe pull load history. By studying the database of installations and considering additional data such as soil type, installation profile, and construction effort, insight can be gained into understanding the probable factors that contribute to total pipe pull load. The installation database can also be used to evaluate the applicability of three current design models, Drillpath (Infrasoft L.L.C. 1996), Driscopipe (Phillips Driscopipe Inc. 1993), and PRCI (Huey et al. 1996). In the following section, model comparisons are made for the simplest case, namely that of the level profile installations. Model comparisons of pulls with significant curvature (pulls 13–15) are not included, as curvature is an additional variable that contributes to pulling loads, and the effect of curvature on pulling loads can best be studied and quantified once the mechanism of load transfer for level profile installations is better understood. The installation database was divided into two sets: (i) level profile installations that were monitored for load only, and (ii) level profile installations that were monitored for combined load and pressure.

Installations monitored for load only

Three models (Drillpath, Driscopipe, and PRCI) were applied to calculate the expected exit pull load for the 12 level installations. These load predictions are compared with the exit pull loads measured by the monitoring cell at the pipe pull head and are summarized in Table 7. Model predictions were calculated for two mud densities, namely 1000 kg/m³ (water) and 1438 kg/m³ (heavy mud with high cuttings content). A friction coefficient for pipe contact with the wetted borehole wall of 0.3 was used for all model calculations, a commonly used industry standard (Maidla 1987). In addition, calculations for the PRCI model were made for two cases, the first assuming zero mud drag and the second a mud drag of 0.35 kPa (0.05 psi converted to kPa). The Driscopipe, Drillpath, and PRCI (zero mud drag) model predictions yield the same results, as they are all based on the same mathematical relationship for straight sections (Baumert and Allouche 2002). The model predictions significantly underestimate the maximum load exerted on the pipe by a factor equal to or greater than 3. When the PRCI model is applied assuming a mud drag of 0.35 kPa, reasonable agreement occurs between maximum pull load model predictions and monitoring cell measurements.

Installations monitored for pull load and mud pressure

The Driscopipe, Drillpath, and PRCI (zero mud drag) predictions of exit load for the HDPE installations, pulls 16 and 17, yield reasonable results. When mud drag of 0.35 kPa is included in the PRCI calculation for these two pulls, the results significantly overestimate actual measurements.

When the Driscopipe, Drillpath, and PRCI (zero mud drag) predictions of exit load are applied to the heavy wall steel pipe installations, pulls 18 and 19, the results significantly underestimate the field measurements. When mud drag of 0.35 kPa is included in the PRCI calculation for these two pulls, reasonable agreement is attained.

Discussion

As the previous results demonstrate, current design models are not able to consistently predict the exit loads, even for the relatively simple case of level profile installations (pulls 1–12 and 16–19). In a sensitivity analysis of HDD design models, Baumert and Allouche (2002) demonstrated that the PRCI model is particularly sensitive to the value of the mud drag factor, followed closely by mud weight (buoyancy). Both of these factors are significant in calculating theoretical in-bore load contributions. The following sections discuss the predicted load components associated with these two factors for the installations reported in this paper.

Mud drag

In the PRCI (Huey et al. 1996) model, fluidic drag is defined as dynamic fluid friction that occurs as the pipe moves through the viscous drilling mud trapped in the borehole annulus. Both the Driscopipe and Drillpath models assume that mud drag is negligible (Phillips Driscopipe Inc. 1993; Infrasoft L.L.C. 1996). The mud drag factor of 0.35 kPa assumed by the PRCI model corresponds to a drilling mud with a high drilled solids content (1438 kg/m³). The PRCI model does not provide any reference for the selection of appropriate mud drag coefficients for different weights and types of drilling mud, nor does it indicate how this particular mud drag factor was derived. The contribution of mud drag to the in-bore load is assumed to vary directly with the pipe diameter (i.e., the pipe surface area). As shown in Table 7, mud drag accounts for a significant portion of the total predicted PRCI load.

Buoyancy considerations

The top three entries in Table 8 summarize the theoretical buoyancy effect for the three different pipe products that were used in pulls 1–19, 220 and 273 mm nominal steel and 220 mm nominal HDPE. Net buoyancy is defined as the

Table 7. Level profile maximum pull load model predictions.

Pull No.	Measured exit load (kN)	Calculated regression exit load (kN)	Predicted load (kN)				Drag component
			Driscopipe, Drillpath, and PRCI for mud drag = 0 kPa		PRCI for mud drag = 0.35 kPa		
			Mud density = 1000 kg/m ³	Mud density = 1438 kg/m ³	Mud density = 1000 kg/m ³	Mud density = 1438 kg/m ³	
1	43.7	37.8	5.4	12.6	40.0	47.2	34.6
2	53.8	45.0	8.4	19.4	62.0	73.0	53.6
3	40.3	33.3	5.4	10.5	34.3	39.4	28.9
4	45.0	35.2	5.6	13.1	41.7	49.2	36.1
5	58.4	51.4	6.4	15.0	47.7	56.3	41.3
6	19.9	18.1	2.4	5.5	17.6	20.7	15.2
7	33.4	28.0	4.1	9.5	30.2	35.6	26.1
8	65.3	56.3	6.8	15.7	50.2	59.1	43.4
9	50.4	46.7	5.8	13.5	43.1	50.8	37.3
10	28.6	23.7	3.3	7.8	24.9	29.4	21.6
11	23.2	21.2	2.8	6.5	20.8	24.5	18.0
12	15.9	15.8	2.4	5.7	18.1	21.4	15.7
16 ^a	15.8	9.6 ^b	8.6	14.2	35.9	41.5	27.3
17 ^a	12.9	11.4 ^b	8.8	14.6	36.8	42.6	28.0
18 ^a	41.9	28.0 ^b	0.8	10.9	37.6	47.7	36.8
19 ^a	51.3	58.0 ^b	0.7	9.9	33.9	43.1	33.2

^aMonitored for load and pressure.^bPressure load component removed.**Table 8.** Buoyancy effect on model predictions of in-bore load.

Pull No.	Pipe properties			Buoyancy (kg/m)		Net buoyancy (kg/m)		In-bore load (kN/m) ^a	
	Material	o.d. (mm)	Weight (kg/m)	Mud density =	Mud density =				
				1000 kg/m ³	1438 kg/m ³	1000 kg/m ³	1438 kg/m ³	1000 kg/m ³	1438 kg/m ³
1–15	Steel	220	25.34	37.91	54.52	12.57	29.18	0.04	0.09
16, 17	HDPE	220	12.26	37.91	54.52	25.65	42.26	0.08	0.12
18, 19	Steel	273	60.24	58.56	84.20	-1.68	23.96	0.01	0.07
GR-1	HDPE	508	53.11	202.70	291.50	149.60	238.40	0.44	0.70
GR-2	HDPE	660	76.48	342.10	492.00	265.60	415.50	0.78	1.22

^aIn-bore load calculated with wet friction coefficient of 0.3.

buoyant force acting on the pipe, less the pipe weight. A positive net buoyancy value indicates that the pipe bears on the crown of the borehole, and a negative value indicates that the pipe bears on the bottom of the borehole. Because of the offsetting effects of buoyancy and pipe weight, the larger and heavier 273 mm steel pipe has the smallest resultant net buoyancy and consequently the smallest predicted contribution to in-bore load. The lighter 220 mm HDPE pipe has a net buoyancy greater than the heavier 220 mm steel pipe and consequently a higher predicted contribution to in-bore load. These examples demonstrate the significance of pipe weight in determining net buoyancy effects for similarly sized pipes. To demonstrate the marked effect that changes in pipe diameter have on net buoyancy and thus total load predictions, two installations (GR-1 and GR-2) from a crossing of the Grand River in southern Ontario are also included in Table 8. In this case a 30% increase in pipe diameter from 508 mm to 660 mm leads to a 78% increase in the calculated

contribution to in-bore resistance for a mud density of 1000 kg/m³ (from 0.440 to 0.781 kN/m) and a 74% increase for a mud density of 1438 kg/m³ (from 0.702 to 1.223 kN/m). Although the PRCI model predicted the maximum load for the larger 660 mm pipe to be approximately double that of the smaller 508 mm pipe, in actuality a 15% increase was recorded in the field. An explanation for this discrepancy may be that the assumption of full buoyancy inherent in all models is incorrect, with the result that the accuracy of model predictions may be seriously affected.

Summary and discussion

Model assumptions: ideal bore conditions

A design model should be universal in its application. The fact that current design models for HDD crossings fail to consistently predict the exit load for 19 level profile installations indicates that the assumptions on which these models

are based are questionable. The following assumptions are common to all three models: (i) a clean stable borehole equal in dimension to the largest reamer used in the construction process; (ii) buoyancy equal to the pipe's volume of displaced drilling mud; and (iii) clear, unobstructed mud flow in the annular space between the pipe and borehole wall. The PRCI model has the added assumption that a significant portion of the total pull load can be attributed to dynamic fluid friction that occurs as the pipe moves through the viscous drilling mud trapped in the borehole annulus.

For economic reasons the majority of HDD installations are not ideal bores. The effort to create a clean stable bore is simply not worth the added time and expense when successful bores can be completed with less than ideal borehole conditions. Installation success is ensured by a combination of adequate pipe strength, a fair borehole condition, and excess rig capacity. Current design models make no provision for the fact that many bores depart from the ideal borehole condition.

Actual bore conditions

A substantial portion of the annular space in many bores can be partially filled with drill cuttings that were not removed from the bore. In these cases annular flow may not be maintained, with mud flow restricted to rivulets within the annular space. In more severe cases, the fluid volume in the bore may actually be less than the pipe volume, with the result that pipe buoyancy is reduced. Under such conditions, the ideal model assumption of buoyancy equal to the pipe's volume of displaced drill mud is incorrect.

The PRCI model, with the assumption of mud drag, provides a mechanism to account for pipe resistance in the bore over and above that which can be theoretically accounted for by net buoyancy effects. The drawback for designers, as mentioned before, is that no values are available for muds of different densities and composition. Furthermore, the conflicting claims that mud drag is negligible (Phillips Driscopipe Inc. 1993; Infracore L.L.C. 1996) need to be resolved with the PRCI claim that it is significant (Huey et al. 1996). Additionally, no provision is made for the possible situation where the volume of displaced solids is greater than the annular space, so compaction of the material in the annular space occurs as the pipe advances. Conceptually, both buoyancy and mud drag are functions of the percentage and composition of soil cuttings left in the bore. The following section proposes a modification to existing design models that takes these considerations into account.

Conceptual framework for an improved HDD design model

The ideal bore condition is the basis for the Drillpath, Driscopipe, and PRCI models. Although the PRCI model attempts to account for the effect of viscous drilling mud with the addition of a mud drag component, this parameter is considered independent of the ideal borehole assumption. No current HDD design models make provision for a borehole with high solids content that may result in (i) a reduction in pipe buoyancy when the volume of the mud slurry displaced in the bore is less than the pipe volume; (ii) displacement of solids into the bore annulus with pipe advance-

ment (annular volume greater than volume of displaced solids) that results in a large contact area between the surface of the pipe and solids left in the bore, a surface that will likely increase axial shear stresses on the pipe; and (iii) displacement of solids accompanied by compaction of solids in the bore annulus when the volume of displaced solids is greater than the annular volume; in the case of cohesive soils, additional normal forces and then axial stresses will result due to compression of the soil by the pipe.

The effect of case *i* can be handled by the multiplication of pipe buoyancy by a reduction factor to account for the actual volume of mud displaced. To quantify the effect of case *ii*, a laboratory testing program is required to evaluate the friction between various pipes and a variety of slurries composed of different soils over a range of different slurry densities. A possible approach to model the effect of a large volume of drill cuttings in the bore annulus (case *iii*) could be based on a modified cavity expansion theory, which considers the residual stresses associated with the expansion of an existing cavity (e.g., Yu and Houlsby 1991). The applicability of cases *i-iii* to a particular project can be determined based on the status of the "bore condition," a parameter discussed in the next section.

Bore condition

The resistance to pipe advancement that builds in a bore is a function of the condition of the bore at the beginning of the pullback operation. For the purpose of determining the resistance to pipe advancement in the bore, the following characteristics can be used to define borehole condition: (i) mud slurry density and viscosity, (ii) mud slurry volume as a percentage of pipe volume, and (iii) composition and volume of settled solids in the bore. Depending on the combination of these characteristics, the bore condition can vary from ideal to severe, as described in the following paragraphs.

In the ideal case, corresponding to a clean bore, the percent solids content settled to the bottom of the bore is negligible. The mud slurry is thin and behaves much like water, with annular flow and near-zero mud drag. From the point of view of buoyancy, there is sufficient mud slurry volume in the bore for the pipe to displace its own volume of drill mud. All in-bore pipe resistance in this case is then because of the net buoyancy effect and the contact friction of the pipe with the borehole wall.

In the severe case, the volume of solid cuttings settled in the bore is such that there is not sufficient space for the pipe to advance without first displacing and (or) compressing the cuttings in the borehole annulus. In this case the volume of mud slurry in the bore is less than the volume of the pipe, with the result that the pipe displaces less than its own volume, thereby reducing the buoyancy effect. A large component of the in-bore resistance is caused by axial shear between the displaced cuttings and the pipe, with net buoyancy accounting for a relatively small portion.

Between these two extremes, from ideal to severe, there are an infinite number of in-bore resistance scenarios, with the net buoyancy effect gradually waning as the dominant component of in-bore resistance, giving way to dynamic mud slurry drag and axial shear effects associated with the contact from the drill cuttings settled in the bore.

Accounting for bore condition

The component of the total pull load resulting from moving that part of the pipe outside the borehole along the ground surface is straightforward to estimate and can be calculated based on pipe weight, surface inclination, and an appropriate surface friction coefficient. Incorporating borehole condition into design procedures is a more difficult task.

Figure 14 is a diagram of the forces acting on a straight-line section based on the PRCI model modified to include a new component called CuttingsDrag. The left-end tension T_2 can be computed using the following static force balance relationship:

$$[1] \quad T_2 = T_1 + |Frict| + FluidDrag + CuttingsDrag \pm W_s L \sin(\theta)$$

where T_2 is the tension at the left end of the section required to overcome drag and friction (kN), T_1 is the tension at the right end of the section (kN), Frict is the friction force between the pipe and soil (kN), FluidDrag is the fluid drag between the pipe and viscous drilling fluid (kN), CuttingsDrag is the wetted solids drag between the pipe and displaced cuttings (kN), W_s is the effective (submerged) weight per length of pipeline plus internal contents (if filled with water) (kN/m), L is the length of section (m), and θ is the angle of the axis of the straight hole section relative to the horizontal ($^\circ$).

The Frict component is modified by the addition of a new parameter, $f(bc)$ (where bc is bore conditions), that reflects the fraction of the pipe volume of mud slurry actually displaced into the bore annulus. The value of $f(bc)$ will vary from 0 to 1 depending on the percent solids in the bore and the ratio of the pipe and bore diameters:

$$[2] \quad Frict = [f(bc) \times PipeBuoyancy - PipeWeight] \mu_{BORE}$$

where μ_{BORE} is the borehole friction coefficient.

The FluidDrag component is also modified by the addition of a new parameter, $g(bc)$, that reflects the fraction of the pipe surface over which mud slurry flows. The value of $g(bc)$ will vary from 0 to 1 depending on the percent solids in the bore and the pipe and bore diameters:

$$[3] \quad FluidDrag = g(bc) \times PipeSurfaceArea \times \tau_{MUD}$$

where τ_{MUD} is the fluid shear stress for the particular mud slurry and pipe surface roughness coefficient.

A new parameter, CuttingsDrag, is introduced to account for the axial shear between the pipe and drill cuttings displaced into the annulus:

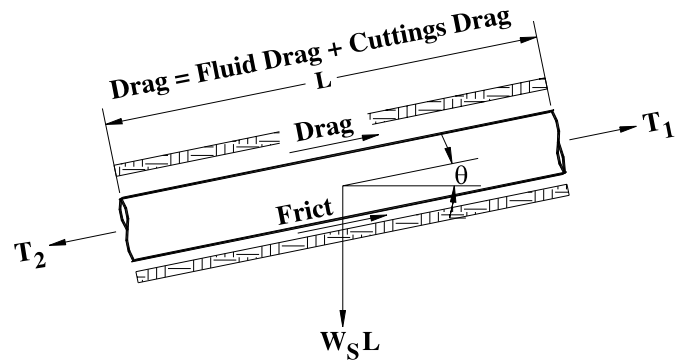
$$[4] \quad CuttingsDrag = [1 - g(bc)] \times PipeSurfaceArea \times \tau(bc)_{CUTTINGS}$$

where $\tau(bc)_{CUTTINGS}$ is the cuttings shear stress. The selected value for $\tau(bc)_{CUTTINGS}$ would be based on the properties of the pipe–cuttings interface, including pressure developed normal to the pipe surface.

Determination of parameter values

To turn the conceptual HDD model presented earlier into a practical design tool, values need to be determined for the

Fig. 14. In-bore pipe resistance for straight section model (modified after Huey et al. 1996).



new parameters $f(bc)$, $g(bc)$, and $\tau(bc)_{CUTTINGS}$ and for the updated variable τ_{MUD} . The authors envision the development of the design model in two stages. First, an empirical design table will be developed, specifying force per unit length for different soil conditions (described in more detail later in the paper). Second, later laboratory and field tests would be used to arrive at a semi-empirical model.

Stage 1: empirical design table of in-bore resistance values

The results from the 12 level installations completed in silty clay indicate that in-bore resistance is related to soil type and level of construction effort. The average in-bore resistance for these 12 bores was 0.26 kN/m ($\sigma_x = 0.03$ kN/m). Further similar field evaluations need to be conducted to determine representative in-bore resistance values for other combinations of pipe type and diameter for different soils and levels of construction effort. To initially structure this process, four broad soil groups are defined (gravelly, sandy, silty, and clayey), and three levels of construction effort (high, medium, and low) are defined as follows:

- (1) High level — High is defined as the construction effort required to ensure a clean, stable bore (near to the ideal condition). The goal is to minimize the level of solids remaining in the bore, thereby minimizing the installation load per unit length of pipe installed. A high level of construction effort would be required in an installation where a clean, stable bore is essential to the successful completion of the pipe pullback. This situation arises in practice when the combination of length of pull, soil, and pipe product could, in the absence of a high level of construction effort, lead to pull loads that exceed the capacity of the rig or the tensile capacity of the pipe.
- (2) Medium level — Medium is defined as the construction effort required to ensure an economic bore. A level of solids accumulation in the bore associated with intermediate installation load levels per unit length of pipe installed is acceptable, permitting the contractor to reduce drilling and back-reaming times as well as volumes of drilling mud pumped. A medium level of construction effort would be employed where there is no substantial risk of exceeding either the capacity of the rig or the tensile capacity of the pipe or of causing surface heave above the bore path.

Table 9. In-bore pipe resistance (200–300 mm o.d.).

Construction effort	Basic soil type							
	Gravelly		Sandy		Silty		Clayey	
	% Solids removed	In-bore pipe resistance (kN/m)	% Solids removed	In-bore pipe resistance (kN/m)	% Solids removed	In-bore pipe resistance (kN/m)	% Solids removed	In-bore pipe resistance (kN/m)
High	—	—	—	—	—	—	—	0.08
Medium	—	0.4–1.2	—	0.4	—	—	—	0.26±0.03 ^a
Low	—	—	—	—	—	—	—	—

Note: Proposed framework only. The values shown are based on data presented in this paper.

^aBased on 12 installations in silty clay.

- (3) Low level — For a low level of construction effort, the focus is strictly on minimizing drilling and back-reaming times as well as volumes of drilling mud pumped while still achieving a successful bore (one that does not exceed the rig capacity or pipe strength limits). High solids content in the bore and associated high installation load levels per unit length of pipe installed are acceptable. Little effort is made to minimize the risk of surface heave. An operator concerned about consistently driving his rig too hard would only employ a low level of construction effort on shorter installations where the required rig load would be at the low end of his capacity. Low level construction effort should be limited to green-field conditions.

With the benefit of a large database of monitored installations, empirical design charts similar in layout to Table 9 could be generated providing typical in-bore resistance loads for a full range of pipe product types and diameters.

Stage 2: semi-empirical parametric model development

Table 9 outlines the proposal to associate a characteristic range of percent solids removed with each level of construction effort and major soil type. It is conceivable that a calculation method for predicting the percent solids removed construction effort and soil type could be developed and verified with field evaluations. These field evaluations would determine the level of solids removed from the bore by monitoring the volume and solids content of the drilling fluid pumped into the bore and returns recovered from the bore during the pilot bore, pre-ream, and pullback operations. With a reasonable prediction of the percent solids likely to be removed from a bore, the fraction of the pipe volume of mud slurry actually displaced, $f(bc)$, and the fraction of the pipe surface over which mud slurry flows, $g(bc)$, could be estimated. Laboratory testing, supplemented with the data of in-bore resistance levels collected during field installations, would be required to evaluate representative shear stress values for the interface between the pipe and compacted drill cuttings, $\tau(bc)_{\text{CUTTINGS}}$, as well as appropriate fluid shear stress values, τ_{MUD} .

The ultimate goal is to develop a rational design model that would provide the HDD designer with a tool to predict pull loads based primarily on soil type and a specified level of construction effort. Together, these two parameters would define the percentage of cuttings removed from the bore. With the additional input of pipe properties and pipe and bore diameters, in-bore resistance could then be estimated using eq. [1] and combined with the load associated with

moving the uninstalled pipe along the ground surface to yield the total load for any location along the bore.

Summary and conclusions

Monitoring cells for the collection of pull load and mud pressure data were successfully developed and deployed on 19 commercial HDD installations, 15 monitored for load alone and four for combined load and pressure. All data collected exhibited an underlying approximately linear relationship that was modulated by local peaks that tended to dissipate quickly, having only a temporary effect on the underlying linear increase in pulling force with the length of pipe inserted. Many peaks appear to be caused by curvature change, and others may be caused by the presence of borehole obstructions (such as tree roots, boulders, or partial borehole collapse). The resistance to pipe advancement in the bore is strongly influenced by the characteristics of the surrounding soil, with pockets of well-graded sand and gravel causing a significant increase in recorded loads compared with those monitored in silty clay.

The addition of pressure-monitoring capability yielded important additional data. In the four installations monitored for pressure it was found that a significant component of the tensile load measured by the monitoring cell results from a mud pressure load on the face of the pipe pull head. To estimate the actual in-bore resistance to pipe advancement, the force resulting from mud pressure on the pulling head and the drag of the uninstalled pipe along the ground surface must be removed from the total load measured by the monitoring cell. When these contributions are removed, an almost linear relationship is observed between in-bore resistance and the length of installed pipe.

Current design models used to predict pull loads for large multi-million-dollar installations are based on the assumptions of ideal borehole conditions, namely a clean stable borehole filled with low-viscosity drilling mud. In this condition, in-bore resistance results from the net buoyancy effect and resulting bore friction at the point of contact of the pipe and the borehole wall. In reality, borehole conditions are often far from ideal and in these situations the Driscopipe and Drillpath models do not accurately model in-bore pipe resistance. The PRCI model attempts to account for less than ideal bore conditions by adding a mud drag component to account for viscous drag of drill mud with high drilled solids content. The PRCI model does not provide ranges for mud drag as a function of mud type, drilled solids content, and pipe surface roughness coefficient, however, and there is

no indication in what situations the 0.35 kPa value employed in the published PRCI design examples can reasonably be applied. In practice, this mud drag factor of 0.35 kPa is now treated as a constant by HDD designers.

Current models fail to account for installations where a significant portion of the borehole is comprised of solid drill cuttings that are not entrained in the mud flow. In this situation, annular mud flow is not maintained, with mud flow restricted to paths within the annulus. In addition, the total fluid mud volume displaced by the pipe may be less than the volume of the pipe, reducing the pipe buoyancy effect. In severe cases, where displaced solid cuttings are greater in volume than the annular space between the pipe and the bore wall, pipe advancement requires compaction of the soil cuttings within the annular volume.

The data collected in this paper indicate that in-bore pipe resistance is a function of the bore condition at the start of the pullback operation. The bore condition can be defined by the percentage of solids removed from the bore, a function of the level of construction effort and soil type. The first stage of a new design approach has been presented to include consideration of soil characteristics using tabulated values of pulling force per unit length based on extensive monitoring of straight pulls. These representative values of in-bore resistance are provided for pipes of different material, weight, and diameter and for different levels of construction effort. The table given here corresponds to three levels of construction effort (high, medium, and low) and four general soil types (gravelly, sandy, silty, and clayey). Several such values were derived from the field data presented in this paper, and these data would be supplemented using further testing.

To calculate HDD pull loads, the HDD designer would begin by specifying a level of construction effort for a particular soil formation. The two parameters soil type and construction effort would define the percentage of cuttings removed from the bore. With the additional input of pipe and bore diameters, the new parameters $f(bc)$, the fraction of the pipe volume of mud slurry actually displaced, and $g(bc)$, the fraction of the pipe surface over which mud slurry flows, would be determined. Representative values of the cuttings shear stress between the pipe and compacted drill cuttings, $\tau(bc)_{\text{CUTTINGS}}$, and fluid shear stress, τ_{MUD} , would then be selected. With these additional parameters $f(bc)$, $g(bc)$, $\tau(bc)_{\text{CUTTINGS}}$, and τ_{MUD} determined, the in-bore pipe resistance component could be estimated using a design equation. Combined with surface loads, the total pull load for any location along the bore could be evaluated. Curvature effects have been ignored in the formulation presented here but could be included once there is a better understanding of the loads experienced during straight profile installations. It is anticipated that monitoring cell technology together with the conceptual framework presented in this paper will lead to the development of more reliable and effective HDD design procedures in the future.

Acknowledgements

Research presented here has been funded through the Industrial Research Assistance Program in collaboration with Optimum Instruments, Edmonton, Alberta, and by Natural Sciences and Engineering Research Council of Canada (NSERC) discovery grants awarded to Drs. Allouche and Moore. The support of the following contractors is gratefully acknowledged: T.W. Johnstone, London, Ontario; Jim Robinson Contracting Inc., Ailsa Craig, Ontario; and A-van Egmond, Smithville, Ontario. Dr. Moore's position at Queen's University is funded by the Canadian Government through the Canada Research Chairs program.

References

- ASTM. 1998a. Standard practice for dry preparation of soil samples for particle size analysis and determination of soil constants (D-421-85). *In* 1998 Annual Book of ASTM Standards. American Society for Testing and Materials (ASTM), West Conshohocken, Pa.
- ASTM. 1998b. Standard test method for particle size analysis of soils (D-422-63). *In* 1998 Annual Book of ASTM Standards. American Society for Testing and Materials (ASTM), West Conshohocken, Pa.
- Baumert, M.E., and Allouche, E.N. 2002. Methods for estimating pipe pullback loads for HDD crossings. *Journal of Infrastructure Systems*, ASCE, **8**(1): 12–19.
- Huey, D.P., Hair, J.D., and McLeod, K.B. 1996. Installation loading and stress analysis involved with pipelines installed in horizontal directional drilling. *In* Proceedings of the No-Dig 1996 Conference, New Orleans, La., 31 March – 3 April 1996. North American Society for Trenchless Technology (NASTT), Arlington, Va. [CD-ROM].
- Infrasoft L.L.C. 1996. Drillpath: theory and user's manual. Infrasoft L.L.C., Houston, Tex.
- Maidla, E.E. 1987. Borehole friction assessment and application to oilfield casing design in directional wells. Doctoral dissertation, Department of Petroleum Engineering, Louisiana State University, Baton Rouge, La.
- Phillips Driscopipe Inc. 1993. Technical expertise application of Driscopipe in directional-drilling and river-crossings. Technical Note 41, Phillips Driscopipe Inc., Richardson, Tex.
- Polak, M.A., and Chu, D. 2002. Effect of parameters on pipe behaviour in HDD installations. *In* Proceedings of the No-Dig 2002 Conference, Montréal, Que., 28 April – 3 May 2002. North American Society for Trenchless Technology (NASTT), Arlington, Va. [CD-ROM].
- Staheli, K., Bennett, D., O'Donnell, H.W., and Hurley, T.J. 1998. Installation of pipelines beneath levees using horizontal directional drilling. Construction Productivity Advancement Research (CPAR) Program CPAR-GL-98-1, U.S. Army Corps of Engineers Waterways Experiment Station, Vicksburg, Miss.
- Yu, H.S., and Houlsby, G.T. 1991. Finite cavity expansion in dilatant soils: soils analysis. *Géotechnique*, **41**(2): 173–183.